Elsevier Editorial System(tm) for Applied Surface Science

Manuscript Draft

Manuscript Number:

Title: Influence of Ce3+ doping on molecular organization of Si-based organic/inorganic sol-gel layers for corrosion protection

Article Type: Full Length Article

Keywords: GPTMS; MTES; sol-gel; AA1050; NMR; EIS

Corresponding Author: Dr. Michele Fedel, Ph.D.

Corresponding Author's Institution: University of Trento

First Author: Michele Fedel, Ph.D.

Order of Authors: Michele Fedel, Ph.D.; Emanuela Callone; Matias Fabbian; Flavio Deflorian, Full Professor; Sandra Diré, Associate Professor

Suggested Reviewers: Florence Ansart
CIRIMAT-LCMIE , Université Toulouse 3 - Paul Sabatier
ansart@chimie.ups-tlse.fr
Expert of sol-gel, physico-chemical characterization of coatings

Marielle Eyraud
 Madirel département de chimie, Aix-Marseille Université
marielle.eyraud@univ-amu.fr
Experience in surface science and electrochemistry

Carmen Perez Perez
ENCOMAT, Universida de Vigo
cperez@uvigo.es
Experience in surface sceince and electrochemical characterization of sol-gel coatings

Department of Industrial Engineering
University of Trento
via Sommarive 9
38123 Trento (TN)
Italy

Trento, 24th February 2017

Dear Editor,

I am submitting to the journal "Applied Surface Science" the original research paper entitled "*Influence of Ce^{3+} doping on molecular organization of Si-based organic/inorganic sol-gel layers for corrosion protection*", by M. Fedel, E. Callone, M. Fabbian, F. Deflorian and S. Diré.

The paper deals with the physio-chemical effect of different cerium loads on the structure of a sol-gel layer obtained from GPTMS/MTES mixtures.

On behalf of the Authors I hereby declare that the work described in the manuscript has not been published previously and that it is not under consideration for publication elsewhere.

On behalf of the Authors I hereby declare that we have no conflicts of interest regarding this manuscript.

Thank you for considering our work

Best Regards

Dr. Michele Fedel

Highlights:

- The DOC of the sol-gel network decreases with Ce addition until Ce/Si-0,019
- Above Ce/Si 0,039 cages become the main silsesquioxane component
- Ce^{3+} ions do not significantly affect the barrier properties of the coatings
- Cerium ions migrate from the network to the metal oxide/sol-gel interface
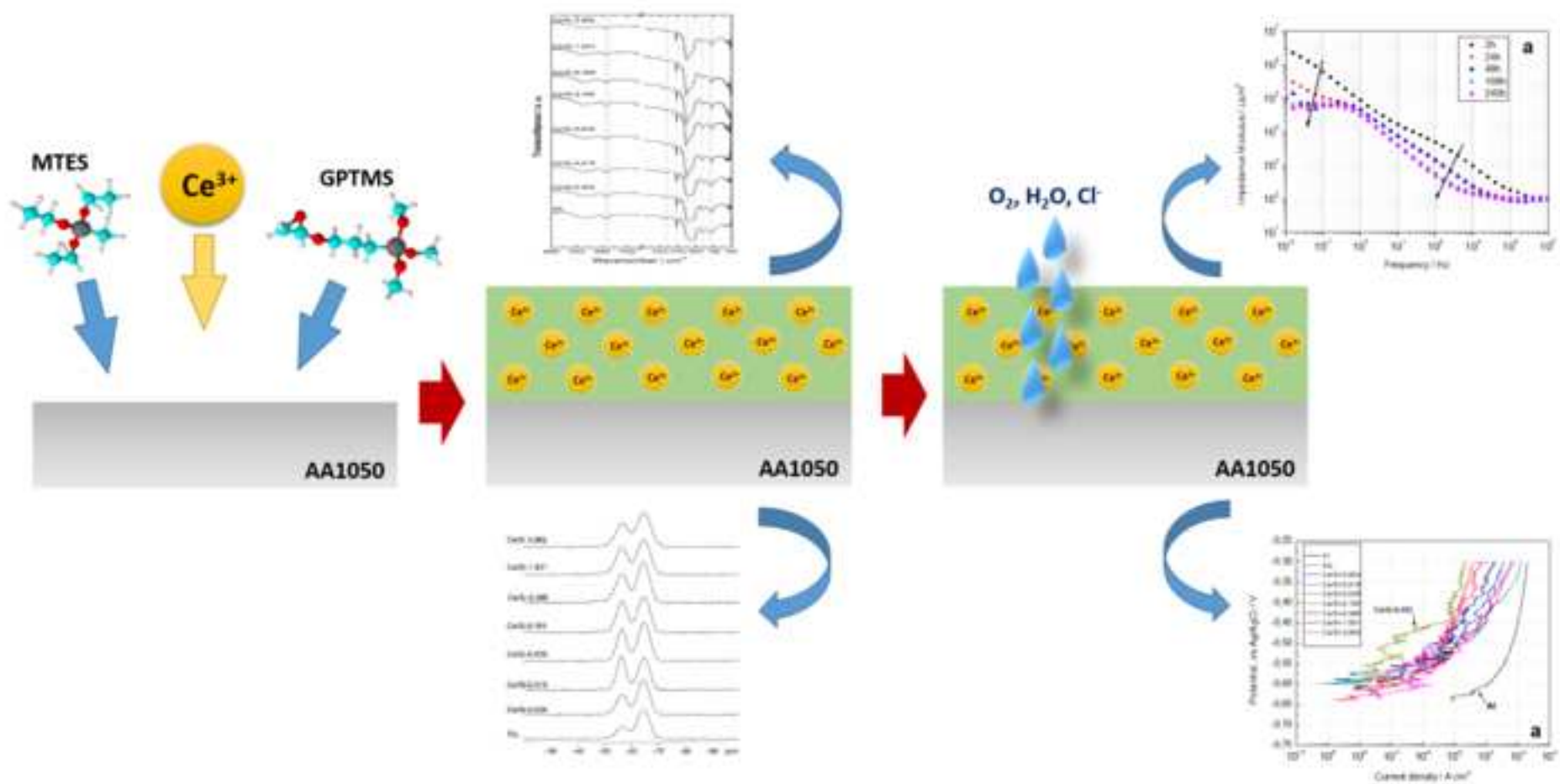
Influence of Ce^{3+} doping on molecular organization of Si-based organic/inorganic sol-gel layers for corrosion protection

Michele Fedel[1,*], Emanuela Callone[1,2], Matias Fabbian[1], Flavio Deflorian[1] and Sandra Dirè[1,2]

[1]*Department of Industrial Engineering, University of Trento, via Sommarive 9, Povo (TN) Italy*
[2] *"K, Müller" Magnetic Resonance Lab, University of Trento, via Sommarive 9, Povo (TN) Italy*
*Corresponding author: michele.fedel@unitn.it

ABSTRACT: In this work, organosilane-derived sol-gel films containing different amounts of cerium ions applied on AA 1050 were investigated. The sol-gel coatings were prepared from 3-glycidoxypropyltrimethoxysilane (GPTMS) and methyltriethoxysilane (MTES) mixtures with the addition of cerium nitrate in order to achieve different concentrations of Ce ions (from 10^{-5} M to 10^{-2} M). The effect of the cerium load on the structure of the cured sol-gel films was investigated by means of solid state NMR and FT-IR spectroscopy. The corrosion protection properties of the different sol-gel layers were investigated mainly by means potentiodynamic curves and electrochemical impedance spectroscopy (EIS). FT-IR and solid state NMR suggested a significant influence of the Ce cations on the network structure: not only the degree of condensation decreases with Ce addition but also the structural modification of the silsesquioxane network is observed with preferential formation of ladder-like species for low Ce^{3+} content and cages predominance for Ce/Si molar ratio greater than 0,039, i.e. [Ce^{3+}] = $1\cdot10^{-4}$ M. Electrochemical tests revealed that the effect of Ce ions on the structure of the coatings do not change remarkably their barrier properties. Moreover, it was found that the Ce ions seems to be present in the cured films and are able to migrate towards the metal/coating interface.

Keywords: GPTMS, MTES, sol-gel, AA1050, NMR, EIS

1. INTRODUCTION

Literature reports that hybrid sol-gel films can be efficiently applied onto different metals to act as adhesion promoters between the metallic substrate and an organic coating [1-10]. In addition, it is also reported that the corrosion protection properties conferred to the metallic substrate by these hybrid layers themselves are noteworthy. In fact, these hybrid coatings are recognized to act as a physical barrier against water and aggressive ion motion to the substrate, thus reducing the extent of corrosion occurring on the metal surface [11,12]. However, these layers do not provide any active

corrosion inhibition of the metal substrate. For this reason, in order to improve the corrosion protection effectiveness of the sol-gel coatings, the addition on many different species and compounds has been proposed. Among them, the addition of inhibitors (inorganic and/or organic) or inhibitor nanocontainers seems to be the most promising strategy to provide the coatings with an effective active corrosion inhibition potential. As far as the inorganic corrosion inhibitors are concerned, particularly interesting to improve the corrosion protection properties of these hybrid layers, is the addition of cerium salts (in particular nitrates and chlorides). Cerium is believed to be an efficient corrosion inhibitor for a significant number of metals and alloys, such as steel, hot dip galvanized steel, tin, aluminum and aluminum alloys, magnesium and magnesium alloy, etc, [13–17]. In fact, because of the local pH increase at the cathodic sites due to the generation of OH^- ions $(2H_2O + O_2 + 4e^- \rightarrow 4OH^-)$, which occurs when a corrosion process takes place, insoluble cerium compounds such as $Ce(OH)_4$ and $CeO_2 \cdot xH_2O$ are formed [18,19]. Moreover, when added in metal alkoxides mixtures, cerium is claimed not only to affect corrosion phenomena occurring at the metal interface but to modify the formation mechanism of the hybrid film as well. However, it is still not clear which is the main effect of cerium addition. J.-B. Cambon et al. evidenced that cerium acts as a network modifier able to affect the condensation rate of the hybrid gel [20]. The same author highlighted that an excess of cerium (>0,01 M) lead to a change in the chemical structure of sol–gel network accompanied by a reduction of corrosion resistance [21]. Similar results were obtained by X. Zhong et al. [22] who evidenced that an increase in cerium content higher than 0,01M decreases the anticorrosion effect of the cerium–silica hybrid coating owing to the decomposition of the silane chains, the increase of Si–OH as well as water adsorption. These findings were partially confirmed by P.S. Correa et al. [23] who sustained that a high Ce ions concentration in the silane film promotes the degradation of the barrier properties of the film, possibly due to the modification of the siloxane network. However, a beneficial effect of Ce ion addition in the silane films due to additional active corrosion protection was recognized in the same work. Accordingly, H.-Y. Su et al. [24] observed an adverse effect of Ce ion on the condensation of the sol resulting in a decrease of compactness of the coating.

It was also hypothesized [25] that cerium is able to promote the hydrolysis of the silane molecules and therefore the condensation of the network, leading to enhanced protective properties of the barrier film. A direct effect of Ce ions on the structure of the sol-gel coating was proposed also by Trabelsi et al. [26], who evidenced that the addition of the lanthanide, as a dopant, improves the barrier properties of the silane coating by increasing the coating resistance and decreasing the coating capacitance. In this case, the author indicated in 0,001M the optimal concentration to optimize the properties of the sol-gel layer. In the same paper it was evidenced that the presence of

cerium ions in the film reduces the corrosion rate of the substrate, Similarly, Zanotto et al. [27] found that cerium ions influence the structure of the silane coating which becomes less porous and defective when about 0,005 M Ce(NO$_3$)$_3$ is added to the deposition bath; moreover, they recognized the contribution of cerium as corrosion inhibitor by promoting a decrease of the overall degradation rate. Other authors [28-30] justified the beneficial effect of cerium in terms of improved corrosion resistance thanks to the presence of the cerium cations that are recognized (1) to affect the reticulation kinetic of the sol-gel and (2) to act as an effective inhibitor at the corroding sites.

On the other hand, V. Moutarlier et al. stated that sol–gel film doping with Ce(III) provides only a weak improvement of corrosion resistance (measured in terms of polarization resistance) of the metal substrate and only for a short term [31]. These results are in accordance with the findings of M. Garcia-Heras et al. [32] who sustained that cerium ions could yield networking defects by the formation of pigment-coating interfaces, which could retain water, while the anticorrosive performance of such doped coatings resides in the inhibitor effect of Ce^{3+} through Ce(OH)$_3$ precipitation. These results were further confirmed by N-C. Rosero Navarro et al. [33] who highlighted that the presence of cerium ions in a sol-gel coating leads to the formation of a porous structure that diminishes the barrier properties. W. Trabelsi et al [34] evidenced that the beneficial effects of cerium doped sol-gel coatings reside mainly in the ability of the lanthanide to accumulates in the stable and protective inner layers of the surface film, providing corrosion protection and self-healing. Similarly, A. Pepe et al. [35] attributed the improvement of coating performance in presence of cerium ions to corrosion products plugging of into the pores and to the inhibition effect of cerium itself, which was recognized to be responsible for cathodic current reduction and a decrease of exposed area as well.

Considering the previously reported literature survey, the effect of cerium ions on the structure of sol-gel coatings derived from Si-based precursors is still object of debate. Generally speaking, it seems that cerium ions have a beneficial effect on the corrosion resistance, increasing the overall protection properties. However, it is not clear if the improved corrosion protection properties are related to the effect of cerium on the sol-gel coating structure or to the corrosion inhibition effect of the lanthanide. In this context, the present work aims at clarifying the role of cerium ions on the structure and corrosion protection mechanisms of sol-gel coatings applied on AA1050 substrate. In particular, both a chemical/physical and electrochemical characterization of the sol-gel coatings were carried out in presence of different concentration of cerium ions in the solution containing the Si precursors. For this purpose, AA1050 samples were dipped into the hydrolysed organosilane solution, prepared from 3-glycidoxypropyltrimethoxysilane (GPTMS) and methyltriethoxysilane (MTES). The effect of different concentration of Ce ions (from 10^{-5} M to $5 \cdot 10^{-2}$ mol/l) on the

structure of the sol-gel film was investigated by means of solid state Nuclear Magnetic Resonance (NMR) and infrared (FT-IR) spectroscopy. The corrosion protection properties of the different sol-gel layers were investigated mainly by means of electrochemical techniques such as potentiodynamic curves and electrochemical impedance spectroscopy (EIS). The tests evidenced that the presence of cerium leads to a modification of the network structure, affecting the degree of condensation. Moreover, it was possible to demonstrate that the anticorrosive performance of cerium ions embedded in the coatings resides in the inhibitor effect of Ce^{3+} at the silane/metal interface while the barrier properties of the coatings seem not to be strongly affected.

2. MATERIALS AND METHODS

2.1 Materials

The organosilane precursors were 3-Glycidoxypropyltrime-thoxysilane (GPTMS, Sigma–Aldrich, 99% purity), and Methyltriethoxysilane (MTES, VWR, 98% purity). These reagents were used as received without further purification. The metallic substrates consisted in a 1050 aluminum alloy (see Table 1). 60 mm × 80 mm plates were cut from the aluminum sheets and were used as a substrate to coat. The samples were degreased with acetone before chemical etching. The chemical etching was performed by dipping for about 60 s the samples in a 25 g/l NaOH solution maintained at 70°C. Cerium ions were added to a water base solution as cerium nitrate hexahydrate ($Ce(NO_3)_3 \cdot 6H_2O$, Sigma–Aldrich, 99% purity). Different concentrations of cerium nitrate were investigated: 0, $1 \cdot 10^{-5}$, $5 \cdot 10^{-5}$, $1 \cdot 10^{-4}$, $5 \cdot 10^{-4}$, $1 \cdot 10^{-3}$, $5 \cdot 10^{-3}$, $1 \cdot 10^{-2}$ mol/l. The pH of the solution containing cerium ions was adjusted to 2,5 by adding hydrochloric acid. The aqueous solution containing the different amount of cerium ions was then added to the silane mixture (5 wt%), prepared with GPTMS/MTES = 1/1 weight ratio. The etched aluminum samples were rinsed in tap water and then in de-ionised water, and were dipped for 2 min in the different silane solutions. The withdraw rate was fixed at 0.2 m min^{-1}. The wet films were cured in an oven for 30 minutes at 160◦C. Table 2 summarizes the investigated samples that were labeled according to their Ce/Si ratio, as used throughout the paper. To perform the solid state nuclear magnetic resonance (NMR) analyses, the silane solutions were deposited onto a PTFE sheet using a tape caster and cured in an oven at 160°C for 30 minutes. The cured films were peeled from the sheet and milled to obtain a fine powder. A coating onto a PTFE sheet was also obtained from a GPTMS/MTES solution, hydrolysed under the same conditions but without cerium addition. After curing and peeling from the substrate, the sample labeled "SIL" was used for comparison.

2.2 Methods

The FT-IR spectra were recorded on a Varian 4100 FTIR Excalibur Series instrument, exploiting the Attenuated Total Reflectance (ATR) geometry in the wavenumber range 4000 - 500 cm^{-1} (32 scans, 4 cm^{-1} resolution) using a diamond crystal as Internal Reflective element (IRE).

The solid state NMR analyses were carried out on a Bruker 400WB instrument working at a proton frequency of 400.13 MHz. NMR spectra were acquired with SP and CP pulse sequences under the following conditions: ^{29}Si frequency: 79,48 MHz, single pulse sequence: $\pi/4$ pulse length 3,9μs, recycle delay 100s, 2k scans contact times: 1 and 5 ms, decoupling length 6.3 μs, recycle delay: 10 s, 5k scans; T_{1Si} were evaluated with saturation recovery pulse sequence. ^{13}C frequency: 100.49 MHz, $\pi/2$ pulse length 3.6μs, recycle delay 5 s, 1k scans, contact time 2 ms, proton decoupling length 6.5 μs, 2k scans. ^{1}H frequency: 400.13 MHz $\pi/2$ pulse 5μs, recycle delay 20s, 16k scans. Samples were packed in 4 mm zirconia rotors, which were spun at 8kHz (11kHz for proton) under air flow. Q_8M_8 and Adamantane were used as external secondary references. The ^{29}Si units were labeled according to the usual T^n notation, where T represents $SiCO_3$ units and n is the number of oxo-bridges.

Electrochemical impedance spectroscopy (EIS) measurements were carried out on the sol-gel coated aluminum samples to evaluate the effect of the different cerium ions concentration on the corrosion protection properties. The impedance spectra were obtained using a PAR Parstat 2273 equipment. A conventional three-electrode cell was used: the working electrode was the investigated sample while a platinum ring and a Ag/AgCl (+207 mV vs SHE) electrode were used as counter and reference electrode, respectively. A Faraday cage was used to minimize external interference on the system. The electrolytic solution was NaCl 0,1 M and the immersed area was about 6 cm^2. The impedance measurements were performed over frequencies ranging from 100 kHz to 10 mHz using a signal voltage amplitude of 10 mV (rms) around open circuit potential (OCP). OCP was measured before starting the collection of the impedance spectra and was potentially maintained during all the measurement time. Using the same equipment and experimental set-up, polarization curves were collected. Anodic and cathodic branches of the curves were separately collected starting from the open circuit potential. A scan rate of 0.166 mV/s was used. All the electrochemical measurements were duplicated to corroborate the experimental results. A Philips XL30 ESEM equipped with an EDS detector was employed to investigate the appearance of the coating after the immersion test.

3. RESULTS AND DISCUSSION

3.1 Sol-gel coatings characterization

The structure of cerium-containing sol-gel coatings was characterized by different spectroscopic techniques in order to detect possible structural changes as consequences of Ce^{3+} addition to the silane mixture. The ^{29}Si NMR analysis was used to focus on the structural features of the silsesquioxane matrix of the coatings. The ^{29}Si CP MAS NMR spectra (Figure 1) of all samples show two peaks, the signal due to fully condensed T^3 units, $RSi(OSi)_3$, at -64,7 ppm and the resonance of T^2 units at -56,6 ppm. According to the ^{13}C NMR results reported below, the latter can be attributed to T^2 species bearing one silanol function ($RSi(OSi)_2OH$). The progressive broadening of the peaks can be observed with increasing cerium content, as a consequence of the addition of a nucleus with paramagnetic character. Neither peaks shift or spinning sidebands increase are detected because, among the paramagnetic ions, Ce^{3+} shows low susceptibility and negligible Fermi contact shift [36,37]. It is worth of noting that the spectra display the increase of T^2 units by increasing Ce/Si molar ratio up to 0,019, then the intensity of T^2 peaks decrease.

The quantitative results were obtained by the profile fitting analysis of the SPMAS spectra (Figure S1, Supplementary Information) that appear pretty similar to the CPMAS spectra. Linewidth (FWHH) and area of peaks are reported in Table 3 (and Figure 2), as well as the degree of condensation (DOC) of the silsesquioxane network, calculated as described in our previous paper [38].

Generally, the DOC value is quite high indicating good crosslinking and structural stability of the films. However, the Ce addition to the silane-based matrix reduces the degree of condensation of the network from 90.9% in the neat silane (Sil) to 88% for Ce/Si-0,004, and then to about 86%, independently on the Ce/Si nominal molar ratio.

Figure 2 highlights the trend displayed by both peak linewidth (Figure 2a) and the amount of the T units (Figure 2b) as a function of the Ce/Si ratio. Low cerium concentrations lead to the decrease in T^3 units and the increase in T^2 units but for Ce/Si nominal ratio higher than 0,019 the relative amount of T^2 and T^3 units appears almost constant. Surprisingly, the linewidth trend shows a minimum for the samples Ce/Si-0.019 and Ce/Si-0.039. With further increasing cerium concentration, FWHH raises continuously, as expected according to the paramagnetic broadening effect. The similar linewidth evolution of T^3 and T^2 units, as well as the observed similarity between CP and SPMAS spectra, suggest that there is no preferential effect of the paramagnetic ion on the different structural T units.

The analysis of the spin-lattice relaxation of the Si nuclei in the different samples was also performed, since theoretically the presence of paramagnetic centres close to the Si nuclei, such as in

6

the case of chelated metal ions, should reduce the T_{1Si} time constant to an extent depending on the concentration of the paramagnetic nuclei [39, 40]. In our samples, the calculated T_{1Si} values (Supplementary Information, Figure S2) do not depend on the cerium concentration and show large scattering like in the case of physical mixing [39], therefore excluding chemical interactions leading to preferential close proximity among cerium ions and silicon nuclei in the hybrid networks.

The ^{13}C CPMAS NMR spectra were recorded to get information on the organic functions in the hybrid matrix. The spectra of all the samples (Supplementary Information, Figure S3 with the embedded scheme for carbon atom labelling) reveal the absence of the characteristic signals related to ethoxy (-OCH$_2$CH$_3$) and methoxy (-OCH$_3$) groups that should be found at 59, 18 and 50 ppm, proving the complete hydrolysis of both organosilane precursors. The signals due to the propyl chain in GPTMS (C1, C2, C3) and the Si-CH$_3$ group in MTES can be clearly detected and allow to calculate the experimental ratio between the two precursors, on the basis of the integrated area of Si-CH$_2$- signal (C1) in GPTMS and Si-CH$_3$ peak in MTES. The experimental GPTMS/ MTES ratio is 1/2.14±0.28 and differs from the nominal one (1/1.3) showing a partial loss of GPTMS during the coating preparation for both undoped and Ce-doped samples.

The signals of the epoxy group of GPTMS (C5 and C6), commonly located at 45-50 ppm, are not detectable indicating that the epoxy ring opening took place. It is well known that epoxy opening can lead to several products according to different reaction pathways [41-43]. Accordingly, the formation of diols and polymerized ethylene oxide species appear both reasonable and can be sustained by the observation of the two signals at 64 and 71 ppm [20, 43-45], which appear very sharp due to the intrinsic mobility. These peaks do not present any shift with increasing the cerium amount, thus excluding true chemical interactions with the lanthanide.

However, as observed in ^{29}Si NMR spectra, the addition of the paramagnetic ion leads to the increase in linewidth of all the signals, which becomes significant for Ce/Si ratio higher than 0,019. Moreover, with increasing the cerium content the intensity of the peaks at 64 and 71 ppm appears to decrease to a larger extent with respect to the other peaks in the organic tail of GPTMS. This effect is clearly observable in Figure S4 (Supplementary Information) that shows the evolution of peaks intensity, normalized to the Si-CH2- peak, with increasing the Ce/Si ratio. This result, even if semi-quantitative and affected by the confidence level of the profile fitting procedure, suggests a preferential interaction due to the proximity of the functions created by the epoxy ring opening and Ce^{3+} ions embedded in the matrix, at least for high Ce concentration. Gröbner et al. have already described a similar behavior by doping with Dy^{3+} a DMPC phospholipid membrane; as a matter of fact, they found that the carbon peaks of the organic tails show a different loss in intensity according to the distance from the paramagnetic center [46].

The proton spectra (Figure S5, Supplementary Information) of all samples are characterized by two broad bands whose relative intensity changes with the cerium concentration. As observed for silicon and carbon NMR, the peak broadening increases for high Ce loading. The peak centred at 0.7 ppm is due to H atoms bonded to carbon in methyl and methylene groups belonging to the organic tails in MTES and GPTMS [47]. The lowfield resonance results from the contribution of OH groups of adsorbed water, silanols, diols and probably Ce-OH groups [48]. The lineshape analysis of the OH band confirms that it results from the overlapping of at least four components. According to the literature, the peak at 6.7 ppm could be assigned to strongly hydrogen bonded OH; the component at 5.5 ppm to C-OH groups, formed by epoxide ring opening; the sharp peak at 4.6 ppm can derive from mobile water molecules, [49,40] and the component at 3.5 ppm could be ascribed to weakly bonded OH. [47, 51,52]. The sharp component at 4.6 ppm is clearly visible in the spectra of the neat silane and only in the samples with Ce/Si ratio up to 0.193, and presents changes in sharpness and intensity in the different samples.

By profile fitting analysis of the proton spectra, the overall intensity of OH and CH bands can be calculated. Figure S6 (Supplementary Information) shows the exponential decrease of the OH/CH band ratio with increasing Ce amount. Taking into account that silanol and diol content is constant according to the above reported NMR results, the reduction in intensity of the OH band with increasing Ce content should be related to the other OH components.

Figure 3 shows the FTIR spectra of the undoped and Ce-doped coatings. The broad band in the range 3600-3200 cm^{-1}, assigned to OH stretching vibrations [53] is produced by the overlapped contributions of adsorbed water and silanols

The two peaks at 2936 and 2880 cm^{-1} are due to C-H asymmetric and symmetric stretching vibrations of -CH_3 (MTES) and propyl CH_2 groups (GPTMS). The corresponding bending vibrations can be observed at 1274 cm^{-1} (Si-CH_3) and at about 1410 cm^{-1} (Si-$(CH_2)_3$-).

The Si–O asymmetric stretching vibrations of the silsesquioxane network produce the strong absorption signals in the ranges 1200-1000 cm^{-1}. The Si-OH stretching mode leads to a signal at 915 cm^{-1} and the peaks at 780 and 770 cm^{-1} are attributed to the symmetric stretching vibrations of Si–C and Si–O bonds, respectively [54].

The siloxane band (1200-1000 cm^{-1}) deserves further comments since the relative intensity of the peaks at 1030-1060 and 1112-1140 cm^{-1} gives information on the amount of cyclic/ladder-like and cage-like components in the silsesquioxane network [55-57]. It is noteworthy that the relative intensity of these peaks changes with cerium concentration. For Ce/Si ratio up to 0,019, the intensity of the two peaks is almost comparable, thus indicating the main contribution of ladder-like silsesquioxane species. However, there is a sort of threshold value of Ce concentration

corresponding to Ce/Si ratio equal to 0,039, over which the cage-like component strongly increases with increasing the concentration of the lanthanide. Looking at the evolution of peaks position vs. Ce concentration (Figure S5), the increase in wavenumber of both signals is observed with increasing Ce/Si ratio up to 0,039; for higher Ce content, the high wavenumber Si-O stretching signal presents constant position at the typical value found for polyhedral cages [58] Thus, an indirect effect of cerium can be identified in promoting the formation of close cages, thus acting as a structure-directing agent towards the hybrid network.

3.2 Electrochemical characterization

The corrosion protection properties of the sol-gel film were analyzed by means of potentiodynamic curves. The electrochemical characterization of the neat sol-gel coating (labeled SIL) and the bare aluminum substrate are reported for comparison. The cathodic and anodic branches of the curves related to the investigated samples are reported in Figure 4 (a,b). The curves are quite noisy, due to the relatively high resistance of the sol-gel coatings. As one can observe in Figures 4a, the presence of the sol-gel layer on the aluminum sheets leads to a significant decrease of the anodic current density, regardless of the cerium amount in the coatings. No clear differences among the samples are observable, except for Ce/Si-0,193 sample, which shows the lowest anodic current density. Similar results were obtained for the cathodic currents (Figure 4b): also in this case, a noticeable reduction of the current density was observed, regardless of the cerium presence and amount in the different coatings.

Based on the polarization curves, the effect of cerium ions on the corrosion protection properties is still unclear. In fact, even if it is likely that the presence of cerium does not negatively affect the properties of the protection system, the real role of cerium in terms of corrosion inhibition is not evident from the collected curves. To better highlight the differences among the studied samples in terms of corrosion protection and to emphasize the corrosion inhibition potential of cerium ions, electrochemical impedance spectroscopy (EIS) measurements in 0.1 M NaCl were performed. Figure 5 (a,b) show the impedance modulus ($|Z|$) and phase, respectively, for the bare aluminum. Notice that the impedance spectra are almost stable during the 240 hours of immersion in the electrolyte, reaching about 10^4 Ωcm^2 in the low-frequency range (about 10^{-2} Hz). In Figure 5b it is possible to observe one time constant, which can be attributed to the faradic process occurring at the metal/solution interface.

Figure 6 (a,b) show the impedance modulus ($|Z|$) and phase, respectively, for the neat silane coated sample. The total impedance noticeably increases compared to the bare sample: after 2 hours of immersion the impedance in the low-frequency range is around $10^6 \div 10^7$ Ωcm^2, more than two

orders of magnitude higher than the bare substrate. During immersion time the modulus keeps decreasing, reaching about 10^5 Ωcm^2 after 240 hours of immersion. Considering Figure 6b two time constants are clearly visible: the first, at about 10^3 Hz can be attributed to the coating, while the second, at about $10^0 \div 10^{-1}$ Hz, is likely to be related to the faradic process occurring at the metal/solution interface. Notice that during immersion time the high-frequency time constant ($\approx 10^3$ Hz) disappears and only one time constant is present in the middle frequency range (around 10^1 Hz, like in the case of bare aluminum). This phenomenon probably relies on the progressive degradation of the sol-gel coating, confirmed by the decrease of the shoulder at $10^3 \div 10^2$ Hz in the impedance modulus plot (Figure 6b). Based on the obtained results, the neat silane sol-gel coatings seem to improve the corrosion resistance of the bare substrate. However, after about 240 hours of immersion, the protective properties are significantly affected by the electrolyte.

As an example, of the impedance response of the sol-gel coatings containing cerium ions, Figure 7 (a,b) show the impedance modulus (|Z|) and phase, respectively, for the sample Ce/Si-0,193.

Notice that the total impedance after 2 hours of immersion is around $10^6 \div 10^7$ Ωcm^2, as for the neat silane coating. However, during immersion time the modulus remains almost constant (over 10^6 Ωcm^2) even after relatively long immersion time (240 hours). In this sense, it seems that the presence of cerium in the coatings does not affect the maximum value of the impedance of the protection system but it strongly influences the stability during immersion in the aggressive solution. Like for the neat silane coating, also in this case, two time constants are observed (Figure 7b). The meaning of the relaxation process is believed to be the same of the SIL sample. From Figure 7 it is possible to notice that also in this case the high-frequency time constant ($10^3 \div 10^4$ Hz) disappears during immersion time in the electrolyte. A complete overview and a comprehensive comparison of the evolution of the impedance spectra during immersion time is provided in Figure 8. As one can observe from Figure 8, sample Ce/Si-0,039 and sample Ce/Si-0,193 show the longest durability in the sodium chloride solution. For these samples the impedance modulus in the low-frequency range remains around 10^6 Ωcm^2 even after 10 days of continuous immersion in the electrolyte, thus indicating a reduced extent of corrosion. On the other hand, it is worth to notice that the contribution of the film to the total impedance (frequency time constant) is approximately the same for all the investigated samples. Since the high frequency time constant was attributed to the sol-gel coating, it seems that regardless of the presence of cerium, the durability during immersion does not change significantly This finding suggest that the decrease in degree of condensation (observed by solid state NMR) and the modification from ladder-like to cages structures (observed by FT-IR) promoted by Ce cations addition, seem not to significantly affect the degradation rate of the sol-gel film itself.

Considering the relative stability of the impedance modulus in the low-frequency range, EIS results suggest that the presence of cerium species provides the metal substrate with enhanced corrosion resistance. In fact, even if the coatings are degraded and do not provide the barrier effect anymore, the impedance modulus attributed to the metal/solution interface do not decrease with time, maintaining relatively high values. This phenomenon is believed to rely on the effect of cerium cations embedded in the coating, which is able to migrate from the network to the metal/solution interface to act as corrosion inhibitors, reducing the corrosion rate. The impedance analyses carried out on the other samples doped with cerium revealed that the best results in terms of capability to maintain high impedance values during immersion time are obtained for sample Ce/Si-0,039 and Ce/Si-0,193. For lower and higher cerium amounts, the high impedance values are not maintained for such a long time, thus indicating a lower corrosion protection efficiency. Combining the EIS results with the polarization curves, Ce/Si-0,193 (corresponding to a cerium nitrate concentration of about $5 \cdot 10^{-4}$ mol/l in the silane solution) seems to be the best performing sample in terms of overall corrosion protection properties.

To complete the characterization, SEM images and EDS analyses were collected on the investigated samples. For example, Figure 9 depicts the appearance of the surface of sample Ce/Si-0,193 and the corresponding EDS Ce, C, O, Al and C maps after 240 hours of immersion in the electrolyte. In particular, considering the map of Ce distribution, one can notice that it is homogeneously dispersed in the coating and on the surface of the metal. In correspondence of the white areas in Ce map of Figure 9 (corresponding to Fe-containing intermetallic compounds) a higher amount of cerium is detected. This was attributed to the cathodic nature of the intermetallic particles which promotes a preferential precipitation of insoluble Ce compounds [59]. Accordingly, the experimental results suggest that the Ce cations which are preferentially located in the network close to diols and PEO chains from GPTMS (as highlighted by solid state NMR measurements), migrate to the metal/coating interface providing corrosion inhibition.

4. CONCLUSIONS

The effect of different concentrations of cerium ions into sol-gel coatings obtained from GPTMS and MTES precursors was investigated in order to unravel the actual effect of the lanthanide, since its actual effect as dopant is object of debate in the literature.

Solid state NMR and FT-IR suggested a significant influence of the Ce cations on the network structure of the coatings. While ^{29}Si CP and SPMAS spectra showed no preferential effect of cerium on T^2 and T^3 units, the degree of condensation was found to decrease with Ce addition and stay constant above Ce/Si-0,019. In addition, the analysis of the spin-lattice relaxation of the Si nuclei

excluded chemical interactions leading to preferential close proximity among cerium ions and silicon nuclei in the hybrid networks. On the contrary, ^{13}C CPMAS NMR revealed a preferential interaction among the functions created by the epoxy ring opening and Ce^{3+} ions embedded in the matrix, at least for high Ce concentration. By means of FT-IR it was found that the presence of cerium affects also the architecture of the silsesquioxane species: up to Ce/Si 0,019 mainly ladder-like structures are present in the network, whereas above Ce/Si 0,039 cages become the main component.

The difference in terms of degree of condensation and silsesquioxane species formed were found not to translate into a remarkably different electrochemical response of the sol-gel coatings. All the investigated coatings, regardless of the amount of cerium, showed a similar impedance contribution in the frequency range corresponding to the relaxation process of the films. However, EIS analysis evidenced that when a certain concentration of cerium ions is added to the sol, a passivation of the metal surface occurs thanks to the migration of cerium cations from the coating to the metal/solution interface. This hypothesis was furtherly confirmed by EDXS analysis. The best compromise for the corrosion protection properties was obtained for Ce^{3+} concentration in the GPTMS/MTES sol in the range $1 \cdot 10^{-4} \div 5 \cdot 10^{-4}$ M.. As a matter of fact, these samples showed a remarkable stability of the low impedance values during immersion time in 0,1 NaCl solution. Considering that in the literature different values of Ce concentration able to optimize the corrosion protection of the hybrid sol-gel layers were reported, we believe that a general statement about optimal Ce^{3+} concentration cannot be made since it strongly depends on the hybrid matrix composition.

REFERENCES

[1] E.P. Plueddemann, Silane Coupling Agents, 2nd ed. Plenum Press, New York, 1990.

[2] K.L. Mittal (Ed.), Silanes and Other Coupling Agents, vol. 4, VSP Brill, Leiden, 2007.

[3] K.L. Mittal (Ed.), Silanes and Other Coupling Agents, Vol. 5, VSP, Brill/Leiden,2009.

[4] W.J. van Ooij, D. Zhu, M. Stacy, A. Seth, T. Mugada, J. Gandhi, P. Puomi, Corrosion Protection Properties of Organofunctional Silanes—An Overview, Tsinghua Sci. Technol. 10 (2005) 639–665.

[5] M.N. Sathyanarayana, M. Yaseen, Role of promoters in improving adhesions oforganic coatings to a substrate, Prog. Org. Coat. 26 (1995) 275-313

[6] H. Wang, R. Akid, A room temperature cured sol-gel anticorrosion pre-treatment for Al 2024-T3 alloys, Corros. Sci. 49 (2007) 4491-4503

[7] L. Trabelsi, E. Dhouibi, M.G.S. Triki, M.F. Ferreira, Montemor, An electrochemicaland analytical assessment on the early corrosion behaviour of galvanised steel pretreated with aminosilanes, Surf. Coat. Technol. 192 (2005) 284-290

[8] F. Deflorian, S. Rossi, L. Fedrizzi, M. Fedel, Integrated electrochemical approach for the investigation of silane pre-treatments for painting copper, Prog. Org.Coat. 63 (2008) 338-344

[9] M. Fedel, M. Olivier, M. Poelman, F. Deflorian, S. Rossi, M.-E. Druart, Corrosion protection properties of silane pre-treated powder coated galvanized steel, Progress in Organic Coatings 66 (2009) 118–128

[10] A.-P. Romano, M. Fedel, F. Deflorian, M.-G. Olivier, Silane sol-gel film as pretreatment for improvement of barrier properties and filiform corrosion resistance of 6016 aluminium alloy covered by cataphoretic coating, Prog. Org. Coat. 72 (2011) 695–702.

[11] D. Zhu, W.J. van Ooij, Corrosion protection of AA 2024-T3 by bis-[3-(triethoxysilyl)propyl]tetrasulfide in sodium chloride solution.: Part 2:mechanism for corrosion protection, Corros. Sci. 45 (2003) 2177-2197.

[12] M. Fedel, M. Olivier, M. Poelman, F. Deflorian, S. Rossi, M.-E. Druart, Corrosion protectionproperties of silane pre-treated powder coated galvanized steel, Prog. Org. Coat 66 (2009) 118–128

[13] Y.C. Lu, M.B. Ives, Chemical treatment with cerium to improve the crevice corrosion resistance of austenitic stainless steels, Corros. Sci. 37 (1995) 145-155

[14] M.F. Montemor, A.M. Simões, M.G.S. Ferreira, M.J. Carmezim, Composition and corrosion resistance of cerium conversion films on the AZ31 magnesium alloy and its relation to the salt anion, App. Surf. Sci. 254 (2008) 1806-1814.

[15] C. Motte, N. Maury, M.-G. Olivier, J.-P. Petitjean, J.-F. Willem, Cerium treatments for temporary protection of electroplated steel, Surf. Coat. Technol. 200 (2005) 2366-2375.

[16] A. Conde, M.A. Arenas, A. de Frutos, J. de Damborenea, Effective corrosion protection of 8090 alloy by cerium conversion coatings, Electrochim. Acta 53(2008) 7760-7768.

[17] M.A. Arenas, J. de Damborenea, Protection of Zn–Ti–Cu alloy by cerium trichloride as corrosion inhibitor, Surf. Coat. Technol. 200 (2005) 2085-2091

[18] M. Schem, T. Schmidt, J. Gerwann, M. Wittmar, M. Veith, G.E. Thompson, I.S.Molchan, T. Hashimoto, P. Skeldon, A.R. Phani, S. Santucci, M.L. Zheludkevich, CeO2-filled sol–gel coatings for corrosion protection of AA2024-T3 aluminium alloy, Corros. Sci. 51 (2009) 2304-2315.

[19] M. Fedel, A. Ahniyaz, L.G. Ecco, F. Deflorian, Electrochemical investigation of the inhibition effect of CeO2nanoparticles on the corrosion of mild steel, Electrochimica Acta 131 (2014) 71–78

[20] J.-B. Cambon, J. Esteban, F. Ansart, J.-P. Bonino, V. Turq, S.H. Santagneli, C.V. Santilli, S.H. Pulcinelli, Effect of cerium on structure modifications of a hybrid sol–gel coating, its mechanical properties and anti-corrosion behaviour, Materials Research Bulletin, 47 (2012) 3170-3176

[21] J.-B. Cambon, F. Ansart, J.-P. Bonino, V. Turq, Effect of cerium concentration on corrosion resistance and polymerization of hybrid sol–gel coating on martensitic stainless steel, Prog.Org. Coat. 75 (2012) 486– 493

[22] X. Zhong, Q. Li , J. Hu, X. Yang, F. Luo, Y. Dai, Effect of cerium concentration on microstructure, morphology and corrosion resistance of cerium–silica hybrid coatings on magnesium alloy AZ91D, Prog.Org. Coat. 69 (2010) 52–56

[23] P.S. Correa, C.F. Malfatti, D.S. Azambuja, Corrosion behavior study of AZ91 magnesium alloy coated with methyltriethoxysilane doped with cerium ions, Prog.Org. Coat. 72 (2011) 739–747

[24] H.-Y. Sua, P.-L. Chen, C.-S. Lin, Sol–gel coatings doped with organosilane and cerium to improve the properties of hot-dip galvanized steel, Corros. Sci. 102 (2016) 63–71

[25] M.F. Montemor, M.G.S. Ferreira, Analytical and microscopic characterisation of modified bis-[triethoxysilylpropyl] tetrasulphide silane films on magnesium AZ31 substrates, Prog.Org. Coat. 60 (2007) 228-237

[26] W. Trabelsi, P. Cecilio, M.G.S. Ferreira, M.F. Montemor, Electrochemical assessment of the self-healing properties of Ce-doped silane solutions for the pre-treatment of galvanised steel substrates, Prog.Org. Coat. 54 (2005) 276–284

[27] F. Zanotto, V. Grassi, A. Frignani, F. Zucchi, Protection of the AZ31 magnesium alloy with cerium modified silane coatings, Mater Chem Phys. 129 (2011) 1– 8

[28] P.H. Suegama, H.G. de Melo, A.V. Benedetti, I.V. Aoki, Influence of cerium (IV) ions on the mechanism of organosilane polymerization and on the improvement of its barrier properties, Electrochim. Acta 54 (2009) 2655–2662

[29] M.F. Montemor, M.G.S. Ferreira, Electrochemical study of modified bis-[triethoxysilylpropyl] tetrasulfide silane films applied on the AZ31 Mg alloy, Electrochim. Acta 52 (2007) 7486–7495

[30] A.M. Cabral, W. Trabelsi, R. Serra, M.F. Montemor, M.L. Zheludkevich, M.G.S. Ferreira, The corrosion resistance of hot dip galvanised steel and AA2024-T3 pre-treated with bis-[triethoxysilylpropyl] tetrasulfide solutions doped with $Ce(NO_3)_3$, Corros. Sci. 48 (2006) 3740–3758

[31] V. Moutarlier , B. Neveu, M.P. Gigandet, Evolution of corrosion protection for sol–gel coatings doped with inorganic inhibitors, Surf. Coat. Technol. 202 (2008) 2052–2058

[32] M. Garcia-Heras, A. Jimenez-Morales, B. Casal, J.C. Galva, S. Radzki, M.A. Villegas, Preparation and electrochemical study of cerium–silica sol–gel thin films, J. Alloy Compd. 380 (2004) 219–224

[33] N.C. Rosero-Navarro, S.A. Pellice, A. Dur´n, M. Aparicio, Effects of Ce-containing sol–gel coatings reinforced with SiO2 nanoparticles on the protection of AA2024, Corros. Sci. 50 (2008) 1283–1291

[34] W. Trabelsi, E. Triki, L. Dhouibi, M.G.S. Ferreira, M.L. Zheludkevich, M.F. Montemor, The use of pre-treatments based on doped silane solutions for improved corrosion resistance of galvanised steel substrates, Surf. Coat. Technol. 200 (2006) 4240– 4250

[35] A. Pepe, M. Aparicio, S. Ceré, A. Duran, Preparation and characterization of cerium doped silica sol–gel coatings on glass and aluminum substrates, J. Non Cryst. Solids 348 (2004) 162–171

[36] J. Plévert, T. Okubo, Y. Wada, M. O'Keeffe, and T. Tatsumi, Evidence of 29Si NMR paramagnetic shifts in rare-earth zeolite LSX., Chem. Commun. (2001) 2112–2113,

[37] V.I. Bakhmutov, B.G. Shpeizer, A. Clearfield, "structure of a paramagnetic supermicroporous silica-based material via a multinuclear solid-state NMR monitoring". Magn. Res. Chem. 2007, 45, 118-122

[38] V. Tagliazucca, E. Callone, A. Quaranta, S. Dirè. Effect of functional groups on condensation and properties of sol–gel silica nanoparticles prepared by direct synthesis from organo-alkoxysilanes. Mater. Chem. Phys. 126 (2011) 909–917

[39] R. J. Smernik and J. M. Oades, Paramagnetic effects on solid state carbon-13 nuclear magnetic resonance spectra of soil organic matter., J. Environ. Qual., 31 (2002) 414–420

[40] Sebastien Maron, Geraldine Dantelle, Thierry Gacoin, François Devreux, NMR and ESR relaxation in Nd- and Gd-doped LaPO4: towards the accurate determination of the doping concentration, Phys.Chem.Chem.Phys., 16 (2014) 187-188

[41] P. Innocenzi, C. Fagus, T. Kidchob, M. Valentini, B. Alonso, M. Takahashi, sol-gel reactions of 3-glycidoxypropyltrimethoxysilane in a highly basic aqueous solution. Dalton Trans. 2009, 9146-9152.

[42] P. Innocenzi, A. Sassi, G. Brusatin, M. Guglielmi, D. Favretto, R. Bertani, A. Venzo, and F. Babonneau, A Novel Synthesis of Sol-Gel Hybrid Materials by a Nonhydrolytic/Hydrolytic Reaction of (3-Glycidoxypropyl)trimethoxysilane with TiCl4, Chem. Mater. 13 (2001) 3635-3643

[43] D. Wencel, M. Barczak, P. Borowski, C. McDonagh. The development and characterization of novel hybrid sol-gel- derived films for optical pH sensing. J. Mater. Chem. 22 (2012) 11720-11729.

[44] D. Hoebbel, M. Nacken, and H. Schmidt, A NMR study on the hydrolysis, condensation and epoxide ring-opening reaction in sols and gels of the system glycidoxypropyltrimethoxysilane-water-titaniumtetraethoxide, J. Sol-Gel Sci. Technol., 12 (1998) 169–179.

[45] M. Templin, U Wiesener, H.W. Spiess, Multinuclear solid state NMR studies of hybrid organic-inorganic materials. Adv. Mater. 9 (1997) 814-817.

[46] G. Gröbner, C. Glaubitz, A. Watts, Probing membrane surfaces and the location of membrane-embedded peptides by (13)C MAS NMR using lanthanide ions., J. Magn. Reson., 141 (1999) 335–339.

[47] J. Brus, Solid-state NMR study of phase separation and order of water molecules and silanol groups in polysiloxane networks. J Sol-Gel Sci Technol 25 (2002) 17–28,

[48] H.E. Mason, S.J. Harley, R.S. Maxwell, S. A. Carroll. Probing the Surface Structure of Divalent Transition Metals Using Surface Specific Solid-State NMR Spectroscopy. Environ. Sci. Technol. 46 (2012) 2806−2812

[49] J-B d'Espinose de la Caillerie, M. R. Aimeur, Y. El Kortobi, A.P. Legrand, "Water adsorption on pyrogenic silica followed by 1H MAS NMR". J. Coll. Interf. Sci. 194 (1997) 434-439

[50] Ingrid Span, Ke Wang, Weixue Wang, Yonghui Zhang, Adelbert Bacher, Wolfgang Eisenreich, Kai Li, Charles Schulz, Eric Oldfield & Michael Groll, "Discovery of acetylene hydratase activity of the iron–sulphur protein IspH" Nature Commun. 1042 (2012) 1-7.

[51] J. Trebosc, J. W. Wiench, S. Huh, V. S.-Y. Lin, M. Pruski. Solid-state NMR study of MCM-41-type mesoporous silica nanoparticles. J. Am. Chem. Soc. 127 (2005) 3057-3068.

[52] Liu C.C., Maciel G.E. The fumed silica surface: A study by NMR. J. Am. Chem. Soc. 118 (1996) 5103-5119.

[53] A. Phanasgaonkar, V.S. Raja, Influence of curing temperature, silica nanoparticles- and cerium on surface morphology and corrosion behaviour of hybrid silane coatings on mild steel, Surf. Coat. Technol. 203 (2009) 2260–2271

[54] M. Aparicio, A. Jitianu , G. Rodriguez, A. Degnah, K. Al-Marzoki, J. Mosa, L.C. Klein, Corrosion protection of AISI 304 stainless steel with melting gel coatings, Electrochim. Acta 202 (2016) 325–332

[55] A. Lee Smith, Infrared spectra-structure correlations for organosilicon compounds, Spectrochim. Acta, 16 (1960) 87–105

[56] E. Borovin, E. Callone , F. Ribot, S. Diré, Mechanism and Kinetics of Oligosilsesquioxane Growth in the In Situ Water Production Sol–Gel Route: Dependence on Water Availability. Eur. J. Inorg. Chem. (2016) 2166–2174.

[57] V. Tagliazucca., E. Callone, S. Diré, Influence of synthesis conditions on the cross-link architecture of silsesquioxanes prepared by in situ water production route. J Sol-Gel Sci Technol 60 (2011) 236–245

[58] S. Dirè, E. Borovin, F. Ribot. Architecture of Silsesquioxanes in Handbook of Sol-Gel Science and Technology L. Klein et al. (eds.), Springer International Publishing Switzerland 2016

[59] F. Andreatta, M.-E. Druart, A. Lanzutti, M. Lekka, D. Cossement, M.-G. Olivier, L. Fedrizzi, Localized corrosion inhibition by cerium species on clad AA2024 aluminium alloy investigated by means of electrochemical micro-cell, Corros. Sci. 65 (2012) 376–386

List of Tables

List of Figures

Table 1. AA1050 composition

	Fe	Si	Mg	Mn	Cu	Zn	Ti	Al
wt%	0,4	0,25	0,05	0,05	0,05	0,05	0,03	Balance (≈ 99,50)

Table 2. Labels: Ce/Si nominal molar ratio of the investigated samples

Ce^{3+} concentration (mol/l)	Sample Label
0	SIL
10^{-5}	Ce/Si-0,004
$5 \cdot 10^{-5}$	Ce/Si-0,019
10^{-4}	Ce/Si-0,039
$5 \cdot 10^{-4}$	Ce/Si-0,193
10^{-3}	Ce/Si-0,386
$5 \cdot 10^{-3}$	Ce/Si-1,931
10^{-2}	Ce/Si-3,862

Table 3. Results of the profile fitting analysis of SPMAS spectra.

Label	Ce/Si %mol	T2 FWHH	Area%	T3 FWHH	Area %	DOC
SIL	0	486,18	27,4	494,31	72,6	90,9
Ce/Si-0,004	0,004	494,64	36,1	482,5	63,9	88,0
Ce/Si-0,019	0,019	335,17	41,3	414,68	58,7	86,2
Ce/Si-0,039	0,039	350,3	41,0	398,4	59,0	86,3
Ce/Si-0,193	0,193	382,68	40,6	448,97	59,4	86,5
Ce/Si-0,386	0,386	452,22	40,5	456,24	59,5	86,5
Ce/Si-1,931	1,931	449,32	42,3	464,93	57,7	85,9
Ce/Si-3,862	3,862	533,85	40,9	489,15	59,1	86,4
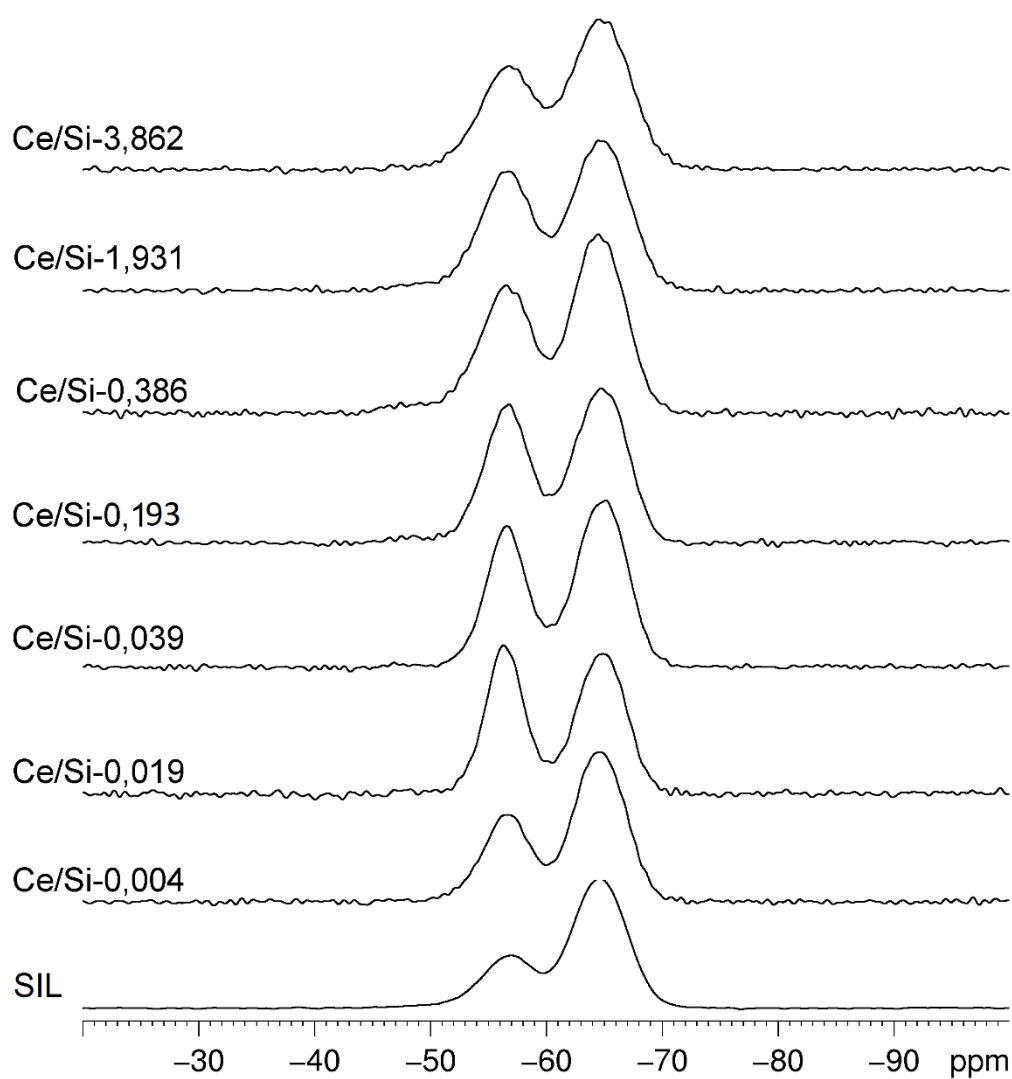
Figure 1. ^{29}Si CPMAS spectra of the samples

1

a)

b)
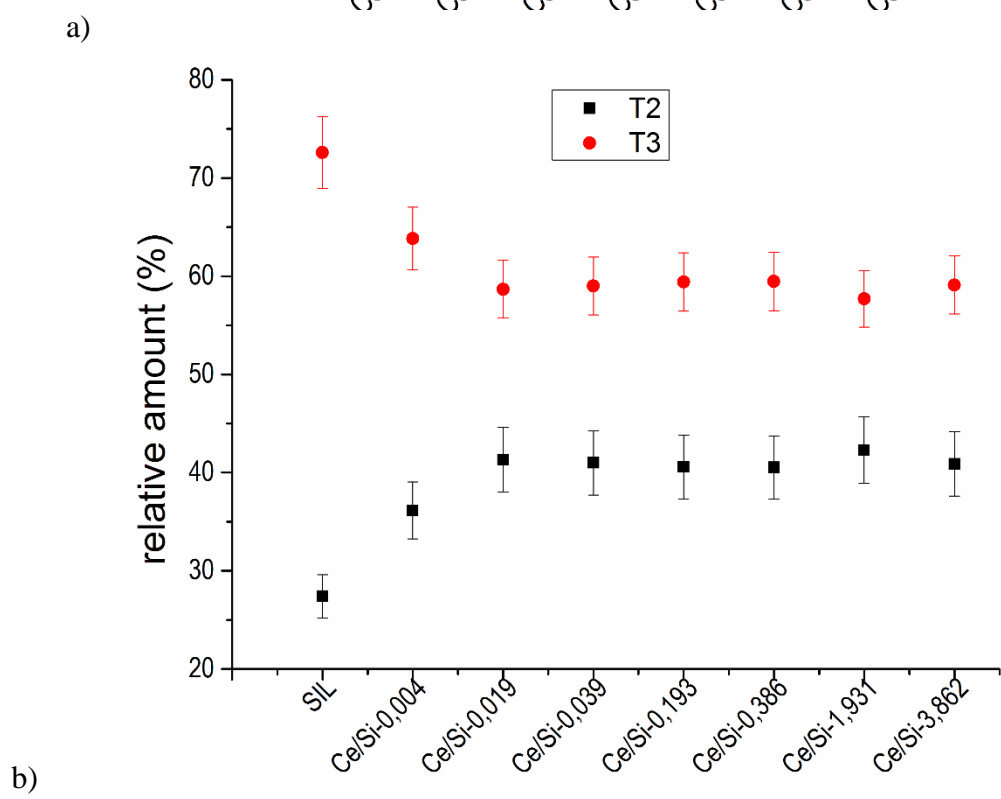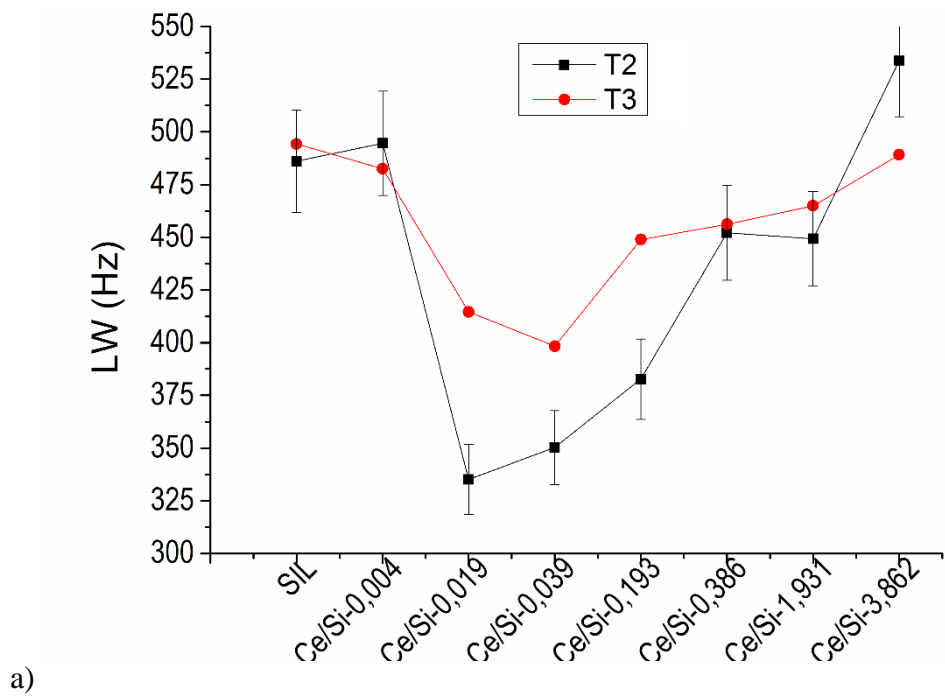
Figure 2. T^2 and T^3 peaks linewidth (a) and area (b) as a function of Ce/Si nominal molar ratio, according to the results of Table 3.
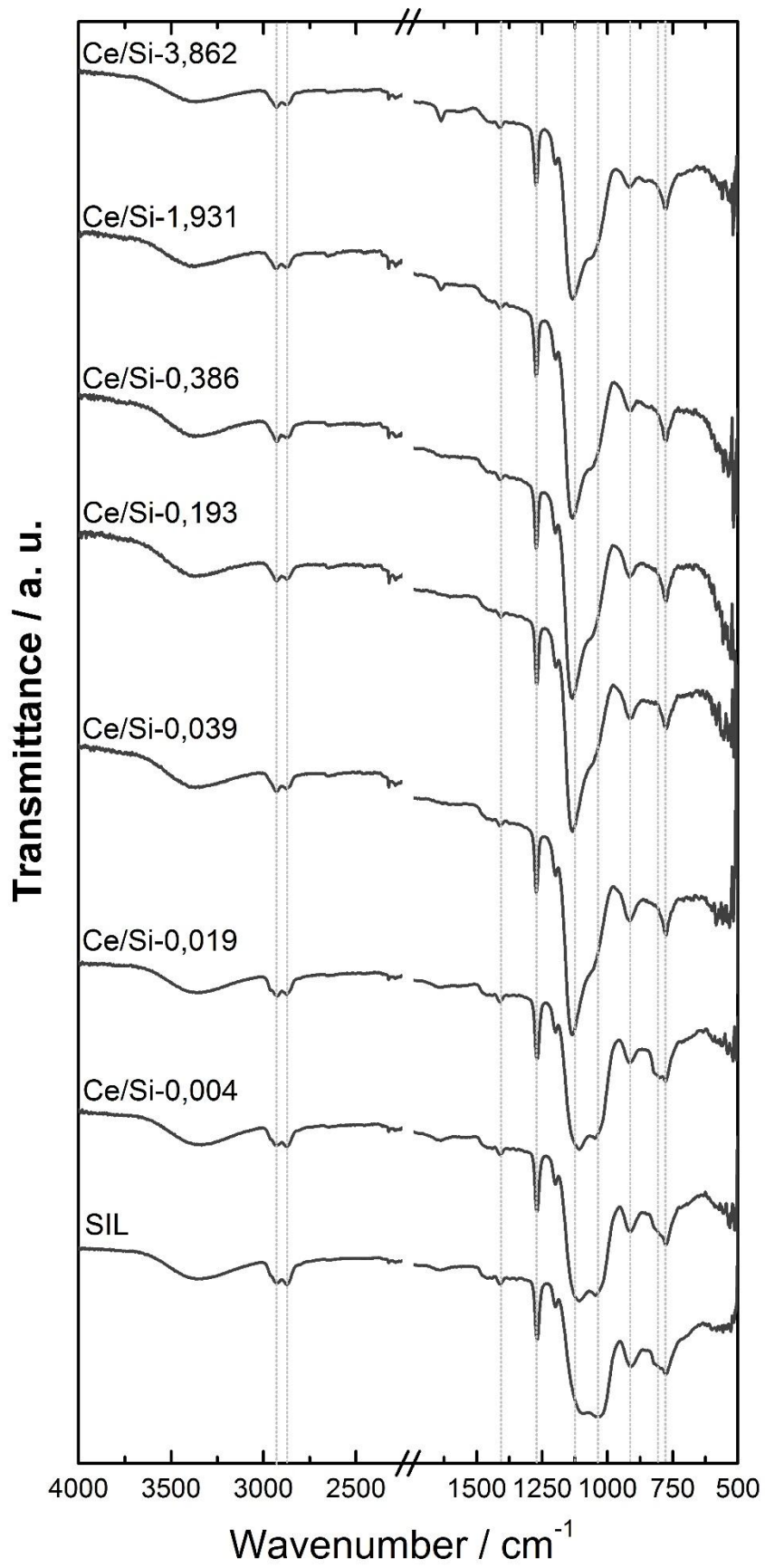
Figure 3. FTIR spectra of neat silane and cerium doped samples

Ce/Si-3,862

Ce/Si-1,931

Ce/Si-0,386

Ce/Si-0,193

Ce/Si-0,039

Ce/Si-0,019

Ce/Si-0,004

SIL

Transmittance / a. u.

Wavenumber / cm^{-1}

4000 3500 3000 2500 1500 1250 1000 750 500
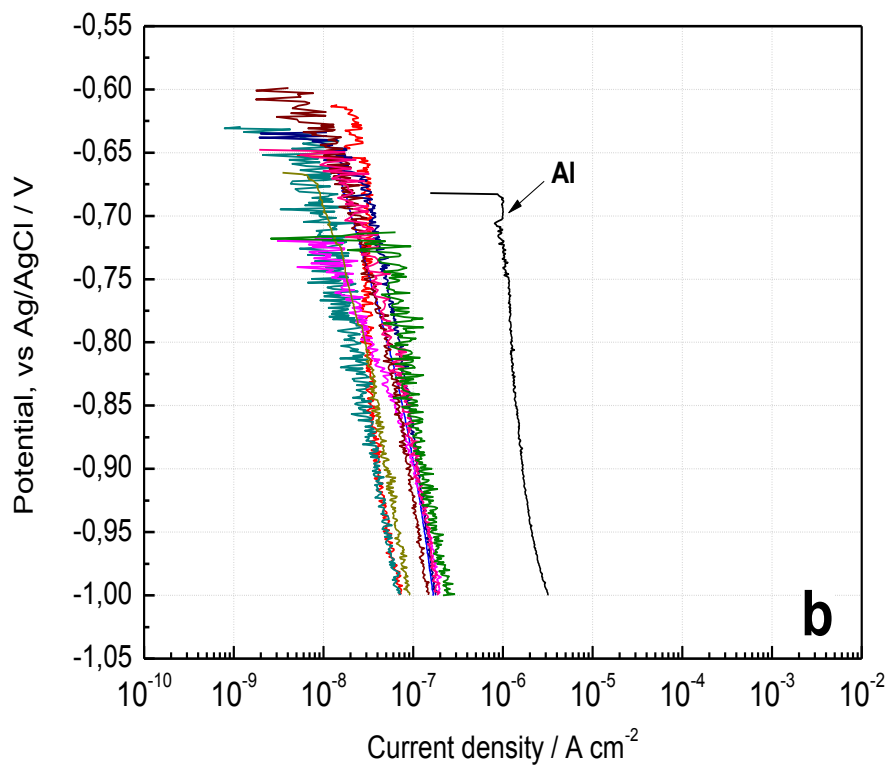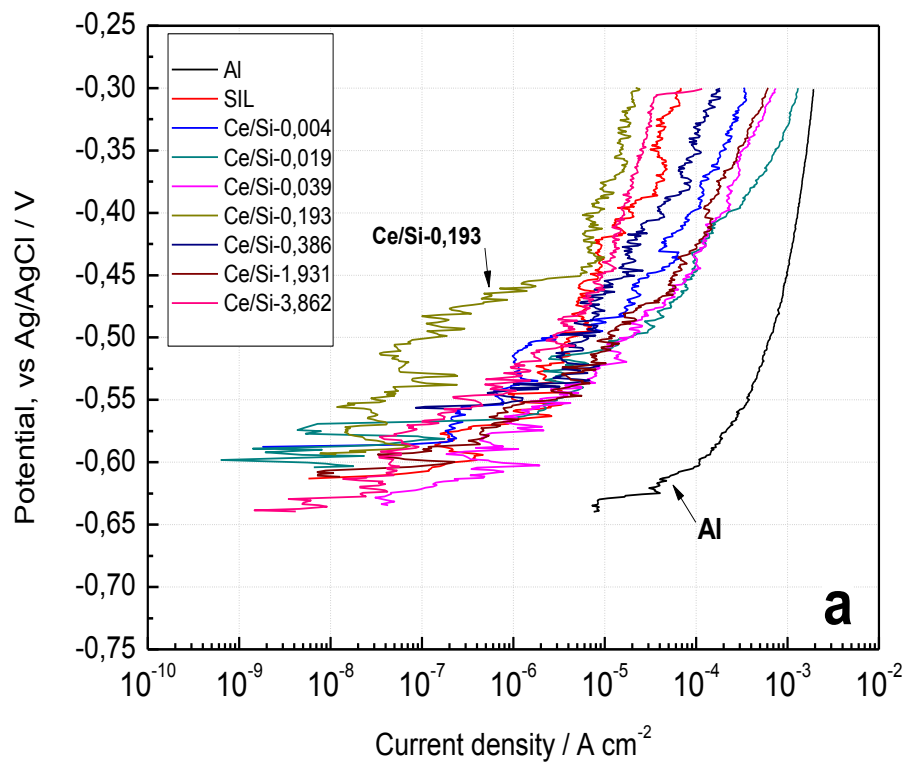
Figure 4. Anodic (a) and cathodic (b) branches of the polarization curves
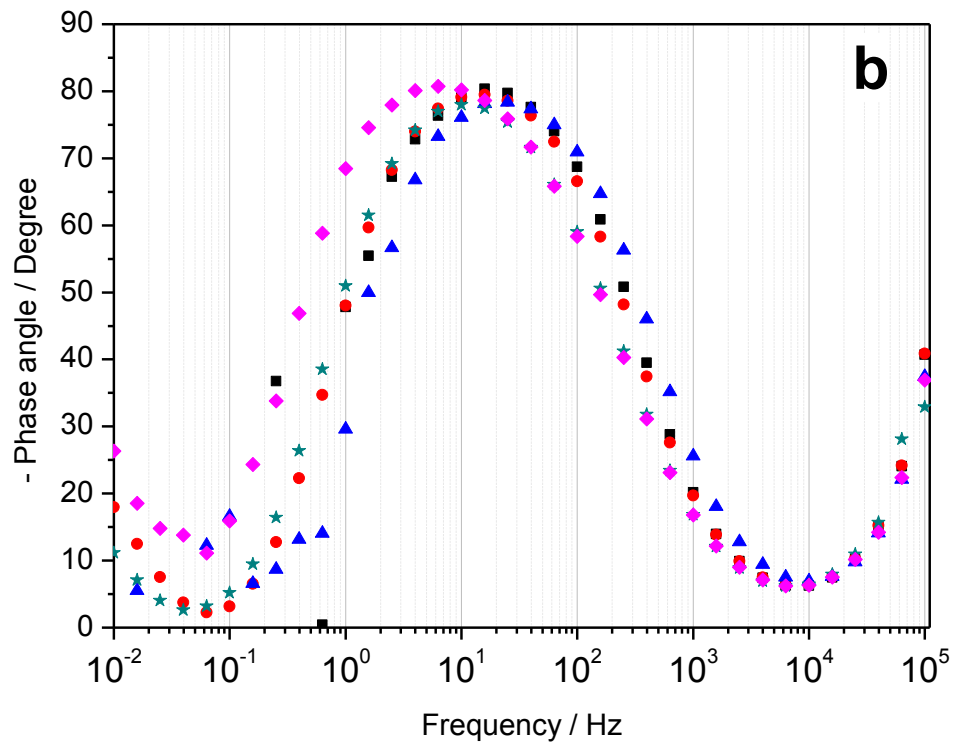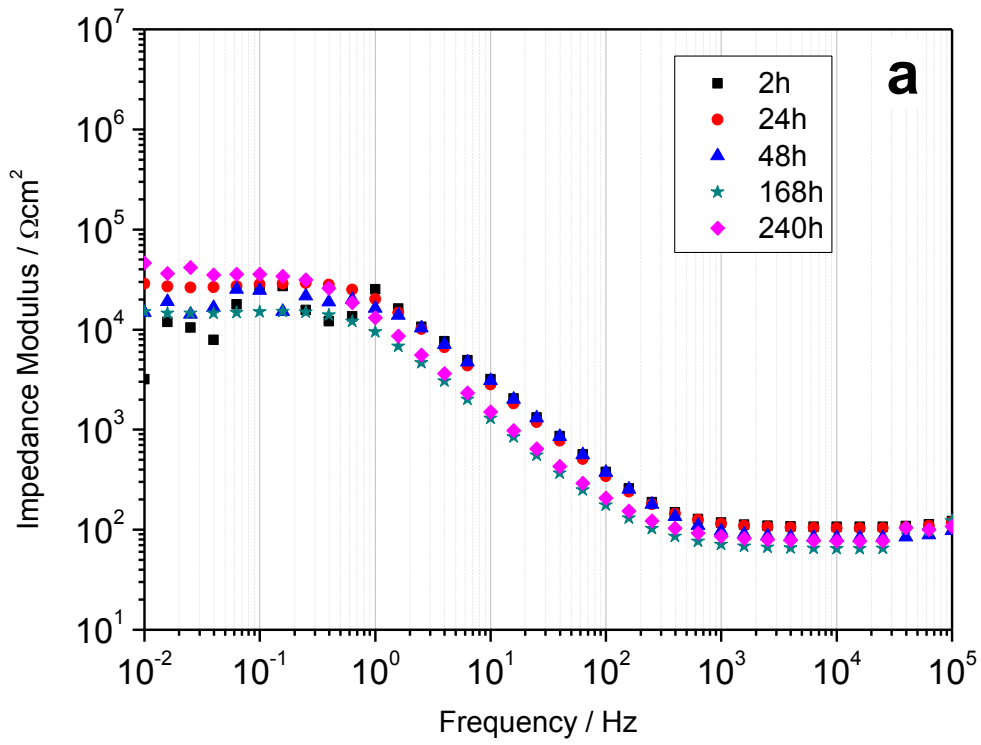
Figure 5. Impedance modulus (a) and phase (b) of bare Al during immersion
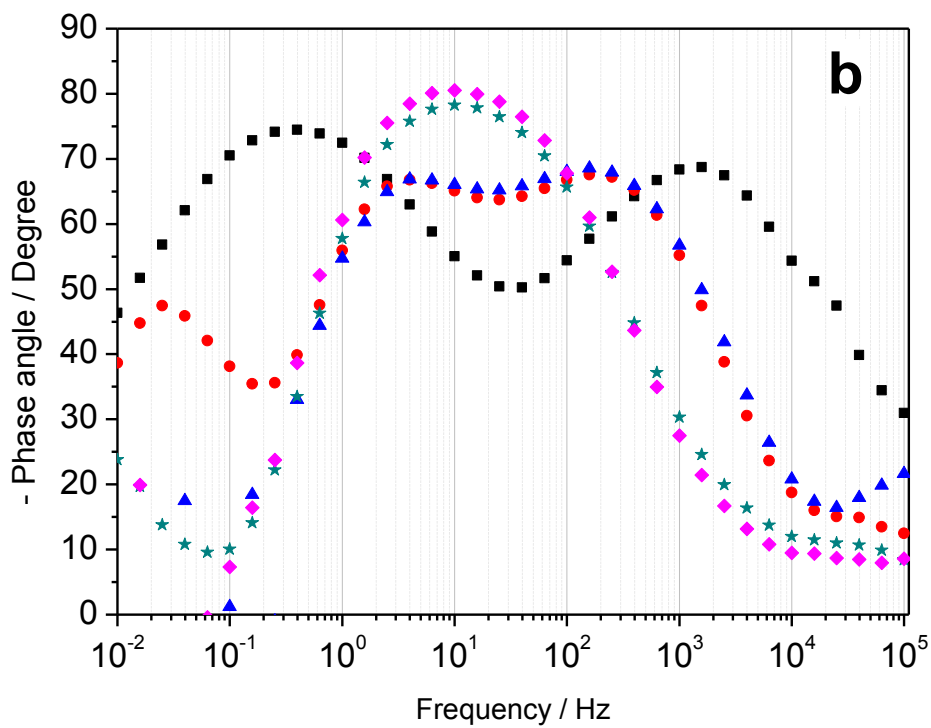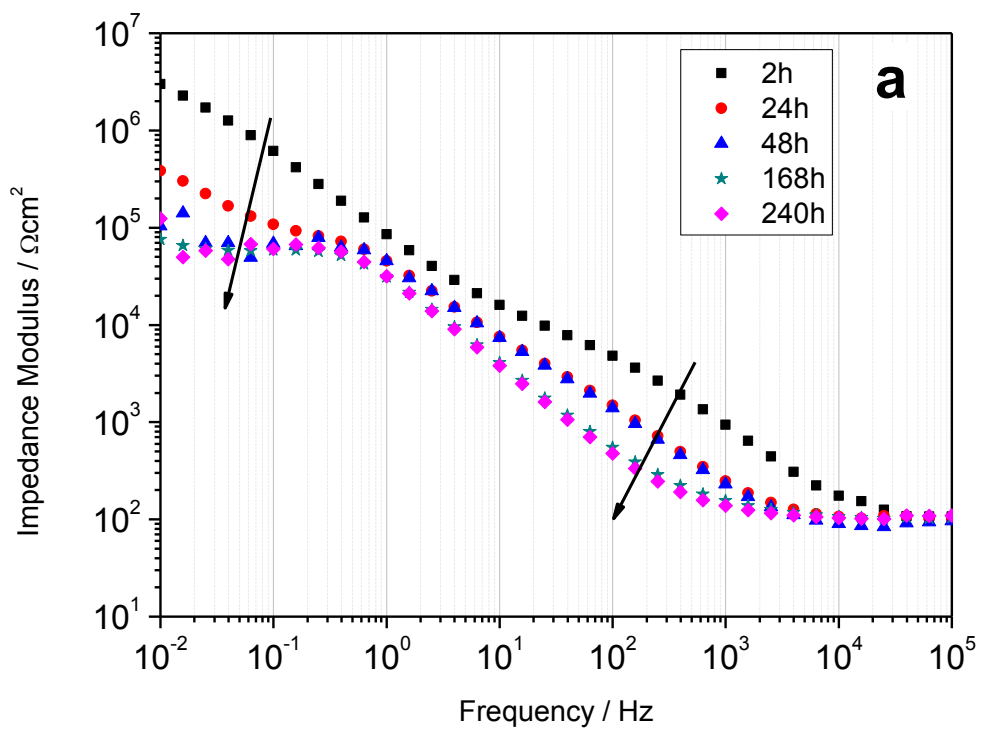
Figure 6. Impedance modulus (a) and phase (b) of neat silane during immersion
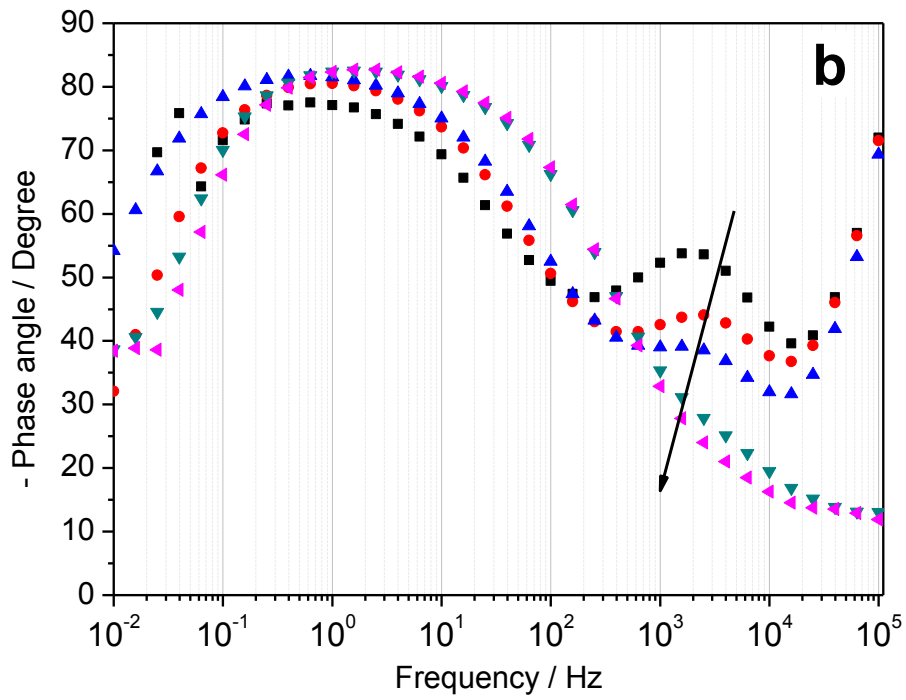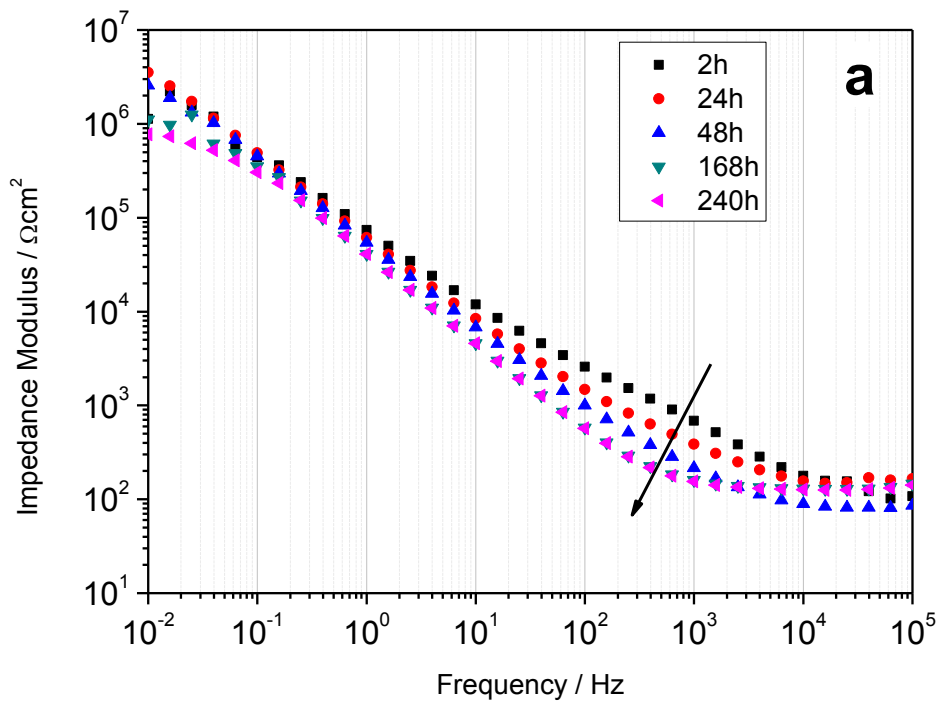
Figure 7. Impedance modulus (a) and phase (b) of Ce/Si-0,193 during immersion
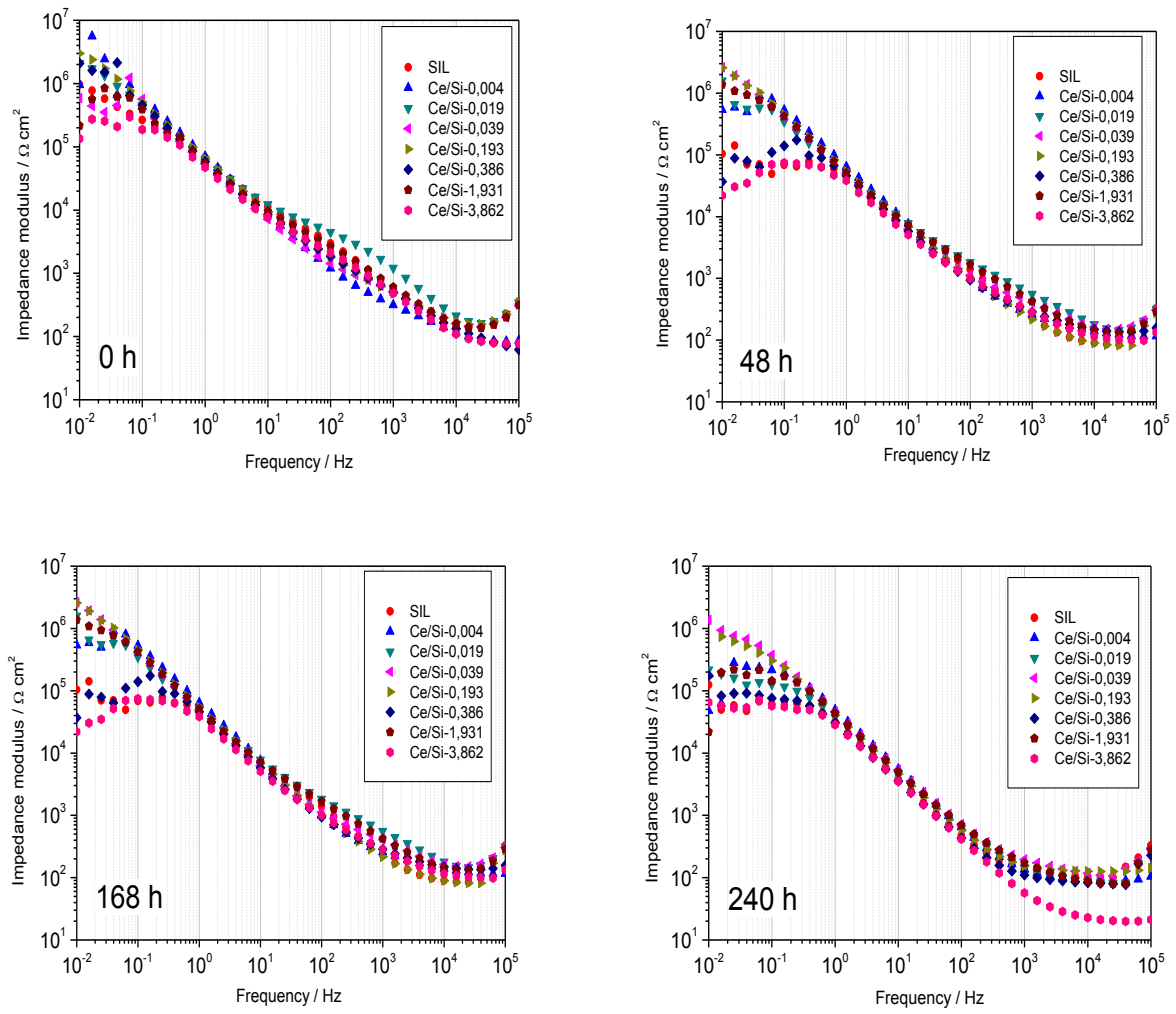
Figure 8. Evolution of impedance modulus during immersion for the investigated samples
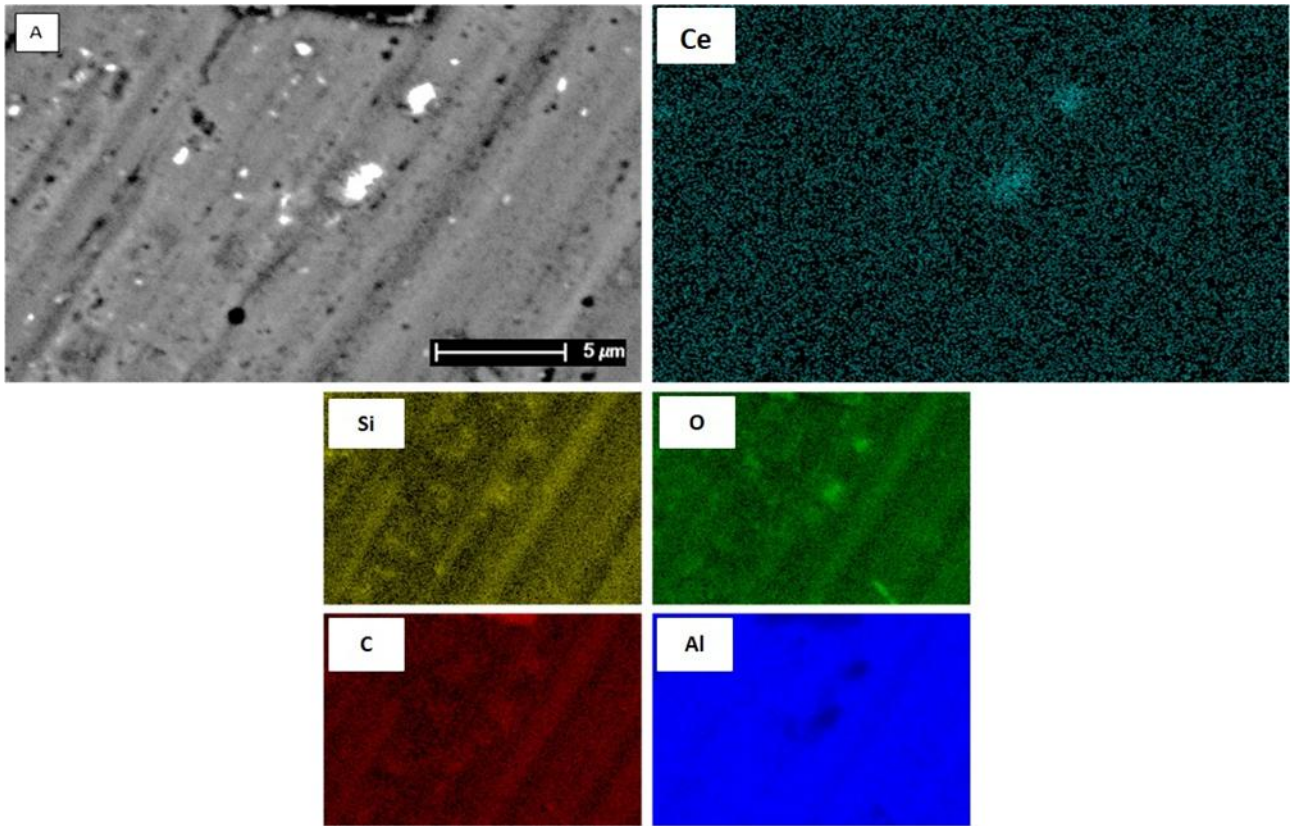
Figure 9. Ce/Si-0,193 surface after 240 hours of immersion in 0,1 M NaCl: surface appearance and EDXS maps

Supplementary Material for on-line publication only
Click here to download Supplementary Material for on-line publication only: Supplementary Information.docx